Exchange bias caused by field-induced spin reconfiguration in Ni-Mn-Sn

A. Çakır,[1,2,*] M. Acet,[2] and M. Farle[2]
[1]*Muğla University, Department of Metallurgical and Materials Engineering, 48000 Muğla, Turkey*
[2]*Faculty of Physics, Duisburg-Essen University, D-47048 Duisburg, Germany*
(Received 29 October 2015; revised manuscript received 25 February 2016; published 9 March 2016)

Exchange bias is observed in ferromagnetic/antiferromagnetic (FM/AF) layered stacks and in materials with neighboring ferromagnetic and antiferromagnetic granules. The latter is commonly observed in Ni-Mn-based martensitic Heusler alloys. In general, the exchange-bias effect is identified as horizontally shifted hysteresis loop when the system is field cooled from high temperatures. We report here loop shifts not only under field-cooled but also under zero-field-cooled conditions in magnetically granular martensitic $Ni_{50}Mn_{50-x}Sn_x$ Heusler alloys in the compositional range $13.0 \geqslant x \geqslant 8.9$. Under zero-field-cooled conditions, the initially applied field can carry the system over energy barriers and stabilize a spin-reconfigured state so that a negatively shifted hysteresis loop can also occur here as in the field-cooled state. Spin reconfiguration occurs when the relative size of the AF and FM regions as well as the relative strength of the of AF and FM interactions are in balance.

DOI: 10.1103/PhysRevB.93.094411

I. INTRODUCTION

The magnetism of martensitic Heuslers is a challenging issue that still needs to be resolved. Other than the more-or-less simple ferromagnetism in the high-temperature cubic austenite state, Ni-Mn-X (X: Al, In, Sn, Sb) martensitic Heuslers exhibit complex magnetic interactions in the low-temperature martensite state [1]. The complexity of the magnetism in this state is closely related to the commensurate and incommensurate modulated martensite structures, on which simple long-range magnetic ordering cannot be configured because of geometrical reasons [2]. Therefore, rather than the occurrence of long-range antiferromagnetic (AF) ordering, short-range AF correlations have been observed in both austenite and martensite states by neutron polarization analysis [3]. There is no indication of long-range AF ordering. The data are practically identical to that obtained from a kagome antiferromagnet [4] or spin ice [5], suggesting that magnetic ordering in the martensite state just below the transition temperature is a frustrated antiferromagnet.

A further issue of the magnetic ordering in the martensite state is the reoccurrence of a partial ferromagnetic (FM) below the so-called martensite Curie temperature T_C^M. Unlike the sharp increase in the initial susceptibility below the austenite Curie temperature T_C^A followed by a temperature-independent behavior at lower temperatures, the initial susceptibility below T_C^M shows a gradual increase with decreasing temperature. This behavior is due to the progressive ordering of mixed, short-range AF and FM components and has been revealed by ferromagnetic resonance experiments [6].

The presence of such mixed states has been shown to lead to the exchange-bias effect in martensitic Heuslers [7]. The exchange bias (EB) property, first observed in partially-oxide-coated Co nanoparticles [8], is identified as a shifted magnetic hysteresis loop in FM/AF bilayers [9] or in magnetically granular materials with FM and AF regions [7,10–13]. The EB property carries importance in being relevant to applications such as magnetic read heads [14], permanent magnets [15], and memory cells [16]. Although it is an established phenomena, the underlying mechanism behind it is still a topic of current investigations [17–19] and some aspects are still being newly understood [12,20].

In the EB effect observed in Heuslers, a symmetric double-shifted hysteresis loop is observed when the sample is zero-field cooled (ZFC) through its blocking temperature T_B, while a symmetric, horizontally shifted loop is observed when the system is field cooled (FC) in an external magnetic field. However, this general scenario can be quite different in magnetically granular Ni-Mn-X martensitic Heusler alloys, where no long-range AF ordering occurs as mentioned above. EB effects in $Ni_{50}Mn_{50-x}Sn_x$ alloys in the range $11 \leqslant x \leqslant 17$ at% were studied by Khan *et al.* [10], and it was observed for compounds in the range $11 \leqslant x \leqslant 16$ at%. These compounds exhibit symmetric, horizontally shifted hysteresis loops in the FC case, and the samples in range $12 \geqslant x \geqslant 16$ at% exhibit double-shifted symmetric hysteresis loops under ZFC conditions. In a work performed by Wang *et al.* [21], EB was observed in both FC and ZFC processes for $Ni_{50}Mn_{50-x}In_x$ Heusler alloys in the composition range $11 \leqslant x \leqslant 15$ at% where super-spin-glass (SSG) properties are found. The occurrence of the EB property for the ZFC state is attributed to the superferromagnetic (SF) unidirectional anisotropy formed during the initial magnetization process [21,22]. Therefore, the EB effect in such systems has usually been pictured as FM entities being embedded in an AF matrix. Although this view is very instructive, also for martensitic Heuslers, it disregards the fact that there is no long-range AF ordering in the martensite state of Ni-Mn-based Heuslers, and there is no Néel temperature to cool through: T_C^M is the common ordering temperature of short-range AF and FM components.

In this work, we examine more closely the magnetic properties of the less-investigated compositional region $8.11 \leqslant (e/a) \leqslant 8.25$ where AF interactions gain strength and become more dominant over FM interactions. Mixed FM/AF interactions can show interesting properties in this concentration regime where FM configurations can be strongly pinned by the antiferromagnetism, thus leading here also to EB effects. Here, we show in Mn-rich $Ni_{50}Mn_{50-x}Sn_x$ martensitic Heuslers that the EB effect can give rise to asymmetric magnetization loops

*cakir@mu.edu.tr

at low temperatures, both when the sample is cooled with or without an applied field. We examine the temperature-dependence of the EB effect in the composition range $13.0 \geqslant x \geqslant 8.9$ corresponding to the e/a range $8.11 \leqslant e/a \leqslant 8.25$. Next to the generation of the SF state, particularly at low temperatures, we show that the FC state can be generated directly from the ZFC state at intermediate temperatures without having to apply a magnetic field first from a high-temperature magnetized state.

II. EXPERIMENTAL

$Ni_{50}Mn_{25-x}Sn_x$ ($x = 13.0$, 11.4, 10.1, 8.9 at%) samples were prepared by arc melting of high-purity elements (99.9%) and were annealed under Ar at 1073 K in sealed quartz tubes for five days. They were then quenched in water at room temperature. The compositions and homogeneity of the samples were investigated by using a scanning electron microscope and energy dispersive x-ray spectra (EDXS). The compositional homogeneity of the samples is determined to be within 0.05%; namely, within the limits of accuracy of EDXS. These samples are among those used in our previous study [23], and the details of their crystal structures determined by Rietveld analysis are given therein.

The magnetic-field dependence of the magnetization $M(H)$ was measured in fields up to 5 T with a superconducting quantum interference device magnetometer. $M(H)$ loops were taken under ZFC and FC conditions in the range $-5 \leqslant \mu_0 H \leqslant 5$ T. For all samples $M(H)$ either saturates or retraces at high fields so that only the field-region relative to the EB effect are shown in the figures. For the ZFC case, the samples were first cooled from 380 K down to the measurement temperature under zero magnetic field, and five-quadrant $M(H)$ measurements were performed starting at $H = 0$. For FC measurements, the samples were cooled from 380 K down to measurement temperature under an applied magnetic field. In this case the measurements start at the value of the cooling field and are four-quadrant.

III. BACKGROUND

Before presenting the data, we provide a brief summary of the general magnetic and structural properties of the Ni-Mn-Sn Heusler system collected in Fig. 1. Figure 1(a) shows the dependence of the magnetic moment per atom μ of $3d$ metals and alloys on the valence electron concentration e/a (Slater–Pauling curve), and Fig. 1(b) shows the e/a dependence of the structural and magnetic transition temperatures. M_s is the martensite "start" temperature and T_{IM} refers to the forward intermartensitic transition temperature. T_C^A is the austenite Curie temperature and T_C^M is the onset of mixed FM and AF ordering.

In Fig. 1(a), the thick (red) line represents the behavior of μ of $3d$ metals and alloys in the FM state. The data for Ni-Mn-Sn and Ni-Mn are also included in this figure [23]. μ of Ni-Mn-Sn initially rises with increasing e/a as the d band fills. $e/a \approx 7.75$ corresponds to the 2-1-1 stoichiometric composition $Ni_{50}Mn_{25}Sn_{25}$ for which μ reaches its maximum. At slightly larger e/a, Mn-Mn near neighbors begin to be encountered in the Mn/Sn sublattice so that AF interactions are introduced, and μ begins to drop. This drop continues until the moment nearly vanishes in the FM state and tends to approach the moment of $Ni_{50}Mn_{50}$ in the AF state.

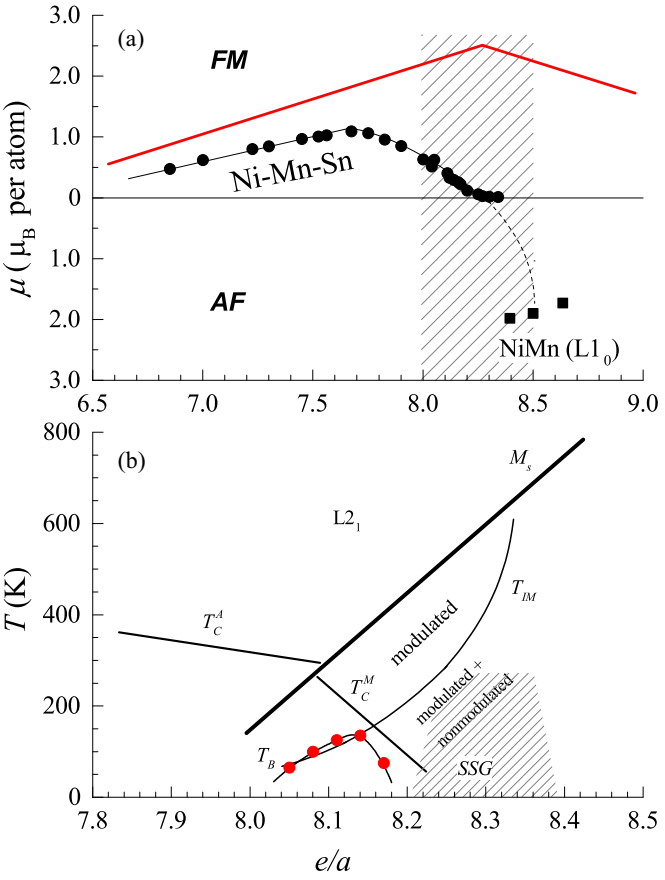

FIG. 1. The magnetic and structural properties of Ni-Mn-Sn Heusler alloys. (a) (e/a) dependence of the magnetic moment. The shaded area is the composition region of interest in the present study. (b) The magnetic and structural phase diagram of Ni-Mn-Sn showing magnetic, martensitic, and intermartensitic transition lines. The regions where blocking and glassy states are encountered are shown with the data points and the shaded region, respectively. All lines are guides.

In Fig. 1(b), we show the structural and magnetic phase boundaries in the region $7.8 \leqslant e/a \leqslant 8.5$ where martensitic and intermartensitic transitions and various types of magnetic interactions occur. Other than the austenite-martensite transition, Ni-Mn-Sn Heuslers also undergo intermartensitic transitions. These occur from a modulated tetragonal phase ($5M$ or $7M$) to a mixture of modulated and nonmodulated ($L1_0$) phases with decreasing temperature [23]. NiMn with $(e/a) = 8.5$ is AF and is $L1_0$. Its Néel temperature T_N lies above the $L1_0$ stability range and is estimated to be about 960 K [24].

Ni-Mn-Sn shows at low temperatures a variety mixed-magnetic interactions as also seen in Fig. 1(b). The alloys up to concentrations $(e/a) \approx 8.34$ do not show any indication of long-range AF ordering [23]. Attempts to determine T_N have shown that, before it can be reached, the austenite state is stabilized. Only SSG states are observed in the range $8.20 \leqslant (e/a) \leqslant 8.34$. Additionally, T_B shown with the (red) data points in Fig. 1(b) is found [10]. Blocking occurs in the

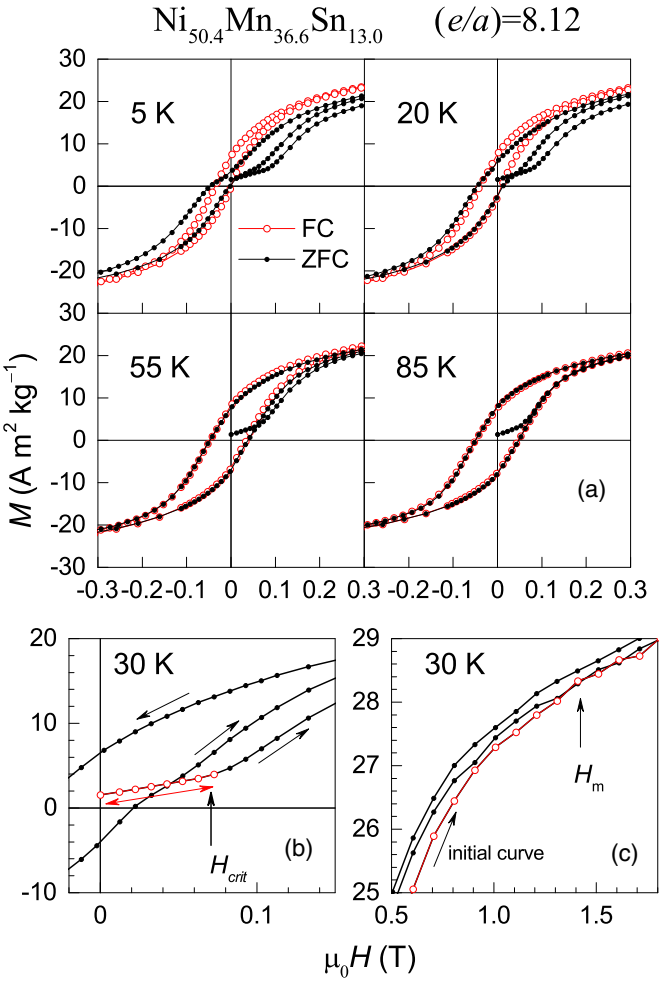

FIG. 2. (a) M-H curves for $x = 13.0$ at various temperatures. Open and closed symbols represent FC and ZFC measurements, respectively. (b) Detailed region showing the definition of $H_{\rm crit}$. (c) Detailed region showing the definition of H_m.

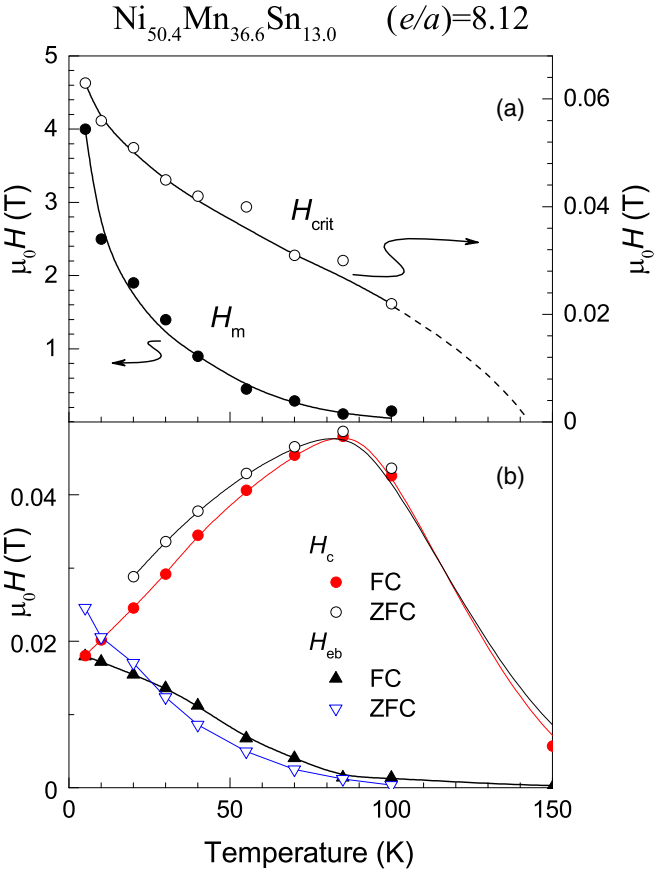

FIG. 3. Characteristic fields for $x = 13.0$. (a) H_m and $H_{\rm crit}$, (b) $H_{\rm c}$ and $H_{\rm eb}$. The lines drawn through the symbols are guides.

range $8.02 \leqslant (e/a) \leqslant 8.20$, where EB effects are observed. The EB effects diminish for $(e/a) < 8.02$.

IV. RESULTS

For EB studies, FC hysteresis loops at low temperatures are usually measured starting at the highest cooling field and then by cycling the field to complete the loop. In the ZFC case, the initial field by nature of the measurement protocol is zero. However, it is very seldom that the initial curve is shown along with the ZFC hysteresis loop because, this curve and the fourth quadrant curve of the hysteresis loop are practically identical, and the double shifted loop is also symmetric around the origin for the compositions $x \leqslant 14.0$ in $Ni_{50}Mn_{25-x}Sn_x$ [7]. At lower Sn concentrations, however, the situation is different, and the initial curve can be located outside the loop, and EB begins to appear also for the ZFC case. We present the data for the individual compounds below.

FC and ZFC hysteresis loops for $x = 13.0$ in the temperature interval $5 \leqslant T \leqslant 85$ K are shown in Fig. 2. The FC loops are symmetric and shifted to negative values up to about 100 K due to the presence of EB. However, unlike conventional EB, the double-shifted hysteresis loops for the ZFC case, particularly at 5 K, are not symmetric about the origin as for $x \geqslant 14.0$ [7]. Both FC and ZFC loops are shifted towards negative fields, and the initial curves lie outside the ZFC loops. $M(H)$ of the initial curve in the beginning increases weakly and almost linearly with increasing field up to a critical field $H_{\rm crit}$. $H_{\rm crit}$ is the field below which $M(H)$ is reversible on applying and removing a field as indicated in Fig. 2(b). Above this field, the initial $M(H)$ curve changes curvature and is no longer reversible along the same path. $H_{\rm crit}$ is therefore the field above which the initial strong pinning effect of the AF exchange begins to be overcome, and the initial state of the systems is no longer recoverable. $M(H)$ begins to increase faster and eventually merges at H_m with the fourth-quadrant branch. $H_{\rm crit}$ and H_m are identified as shown in Figs. 2(b) and 2(c) as examples. At temperatures $T \geqslant 20$ K, the ZFC loop begins to lose its double-shifted character and starts taking a similar shape as the FC loop. For $T \geqslant 70$ K, the FC and ZFC loops are identical.

The EB field $H_{\rm eb}$ and the coercive field $H_{\rm c}$ become practically the same for FC and ZFC loops at these temperatures.

The behavior of the characteristic fields as a function of temperature for $x = 13.0$ are plotted in Fig. 3. Figure 3(a) shows the temperature dependence of $H_{\rm crit}$ and H_m where both decrease with increasing temperature. $H_{\rm eb}$ and $H_{\rm c}$ for the FC and ZFC cases are shown in Fig. 3(b), where both exhibit similar behavior. $H_{\rm c}$ first increases with increasing temperature

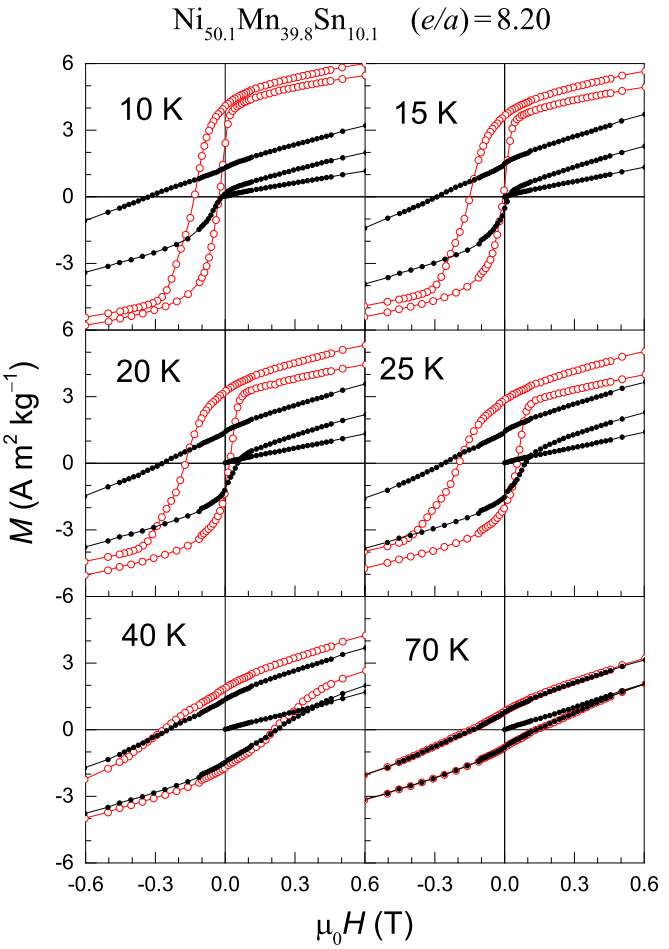

FIG. 4. M-H curves for $x = 10.1$ between 10 and 70 K. Open and closed symbols represent FC and ZFC measurements, respectively.

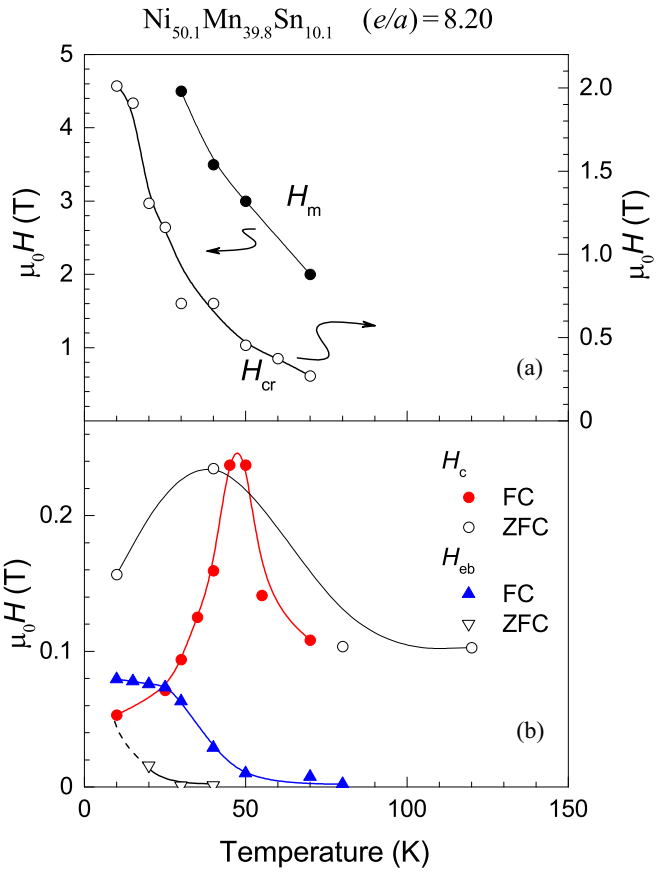

FIG. 5. Characteristic fields for $x = 10.1$. (a) H_m and H_{crit}, (b) H_c and H_{eb}. The lines drawn through the symbols are guides.

both for FC and ZFC loops up to a maximum after which it begins to decrease. The cause of the maximum is related to the competition of AF and FM exchange in a magnetically frustrated state when a thermal energy kT is supplied. At low temperatures where the EB effect is largest, strong AF exchange acts against the effect of FM domain pinning that would normally cause a broad hysteresis and therefore a large H_c. At higher temperatures AF exchange weakens, allowing domain pinning to become more effective and H_c increases to a maximum. Above this temperature H_c begins to decrease with the weakening FM exchange as the temperature further increases and tends to vanish as T_C^M is approached.

The results obtained on a sample with a lower Sn concentration, $x = 11.4$ (not shown here), yield practically the same results for $M(H)$ and the same results for the characteristic fields.

For the sample with $x = 10.1$, both FC and ZFC loops are shifted and are asymmetric around the origin up to about 40 K after which the FC and ZFC loops are identical, as seen in Fig. 4. Up to about 70 K, the initial ZFC curve lies outside the loop, and the characteristic fields all increase with respect to those of $x = 13.0$ and 11.4, as seen in Figs. 5(a) and 5(b). Due to the asymmetry of the loops, it becomes more difficult to define a figure of merit for the characteristic fields. However, it can be seen that they do shift to higher values with respect to those of lower Mn concentrations and that their temperature dependencies remain similar. At 10 K, H_{eb} already reaches large values of about 0.1 T.

The EB effect is still observed in both FC and ZFC cases in $x = 8.9$, as shown in Fig. 6. At 10 K, $H_{eb} \approx 0.25$ T, which is similar to the value reported in Ref. [22] for a compound of similar composition. However, this decreases rapidly with increasing temperature. ZFC EB is still present up to 70 K.

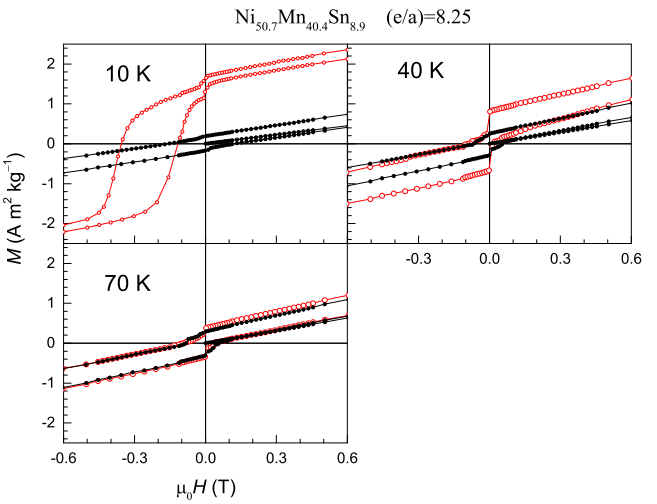

FIG. 6. M-H curves for $x = 8.9$. Open and closed symbols represent FC and ZFC measurements, respectively.

As a general result we find the EB occurs under both FC and ZFC conditions and they persist as long as glassy conditions prevail. Although the magnetic moment drops with increasing Mn concentration, the characteristic fields, particularly H_{eb}, increases at low temperatures.

V. DISCUSSION

A. Magnetization and characteristic fields

In $Ni_{50}Mn_{25-x}Sn_x$, a ZFC EB effect is not found at Sn compositions $x > 13$ [10]. Instead, a regular double-shifted hysteresis loop is observed with no horizontal shift with respect to the origin. In this case, the initial curve and the fourth-quadrant branch of the hysteresis loop cannot be distinguished. The ZFC EB effect begins to be observed for $x \leqslant 13$ where the initial $M(H)$ curve begins to extend outside the main loop. This composition corresponds to the case where the AF exchange begins to percolate through the sample, as discussed in Sec. V B. This critical enhancement leads to a stronger pinning of the initial FM configuration at $H = 0$ causing H_{crit} to acquire a value so that the irreversible part of $M(H)$ extends to fields that are larger than the width of the hysteresis.

The initial curve merges with the fourth-quadrant branch at H_m where the state of the system is completely forced out of the initial ZFC configuration into a new configuration, and the loop does not include the initial curve any more. The curve of the new configuration is shifted with respect to the origin, and the shape resembles that of a double-shifted loop, but with an EB of nearly the same magnitude as that of the FC EB loop. With increasing temperature, H_{crit} decreases, and so does H_m as T_B is approached. The systems is forced out of the initial ZFC state and the EB-bias effect is observed without having to cool the system from high temperatures under an external field. The scenario is similar for $x = 11.4$ and 10.1. Only the magnetic moment decreases with increasing Mn concentration, in accordance with Fig. 1. Although still present in the FC case, the EB effect is essentially lost in the ZFC case for $x = 8.9$.

To provide evidence for the occurrence of spin reconfiguration in the ZFC case we have also measured "backward" hysteresis loops, i.e., by beginning the loop by first increasing the field negatively. We show this as an example for the $x = 11.4$ sample in Fig. 7 for "forward" [Fig. 7(a)] and backward [Fig. 7(b)] hysteresis loops. The loops are seen to be symmetric around the horizontal axis, and a positive shift of the hysteresis is observed. This is an indication that spin reconfiguration is indeed occurring as the field is initially increased. If spin reconfiguration were not occurring, and a remnant magnetization were present, the initial curve would have joined the third-quadrant curve upon applying the negative field and the usual negative EB effect would be observed.

B. Compositional considerations

In $Ni_{50}Mn_{50-x}X_x$ Heusler compounds with Mn-rich compositions, Mn atoms in the Mn-X sublattice can occupy positions where the nearest neighbor can also be a Mn atom so that AF interactions set in. In the case of $Ni_{50}Mn_{50-x}Sn_x$, this occurs at $(e/a) > 7.75$ $(x > 25)$ as evidenced from the onset of

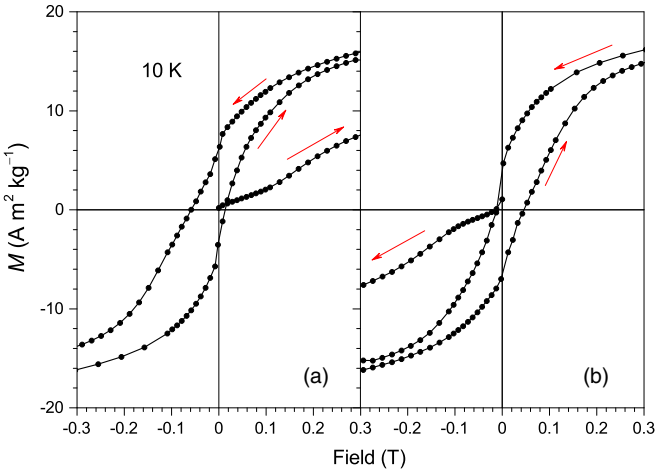

FIG. 7. M-H curves for $x = 11.4$ (a) taken on initially positively and (b) initially negatively increasing fields.

the deviation of the magnetic moment from the Slater–Pauling curve (Fig. 1). At this value, $\mu = 1.1\mu_B$/atom. Although AF interactions begin to be present at this concentration, EB is observed as of $(e/a) = 8.02$ $(x = 16)$ [10]. At this composition $\mu = 0.66\mu_B$/atom, i.e., well off the 2-1-1 stoichiometric composition.

From Fig. 1, no AF exchange is present at $(e/a) = 7.75$ and only AF exchange is present at $(e/a) = 8.50$, i.e., $Ni_{50}Mn_{50}$. Although the average magnetic moment per atom in the unit cell decreases with increasing (e/a), the magnetic moment on the manganese atom remains constant at about $4\mu_B$ [25]. Therefore, the development of AF exchange-coupling occurs essentially without a change of the Mn moment so that one can estimate the relative amount of AF exchange present in the sample by scaling it to the average magnetic moment per atom; namely, by linearly interpolating between the boundary values $1.1\mu_B$/atom for $(e/a) = 7.75$ and $-1.9\mu_B$/atom for $(e/a) = 8.50$. The negative sign for μ is taken for the AF case. The relative amount of AF exchange in the composition range of the interpolation is given in Table I.

The onset of EB at $x = 16$ with $\mu = 0.66\mu_B$/atom requires about 15% of the exchange to be AF. About 37% AF exchange is required for the average magnetic moment to vanish.

A composition of particular interest is $x = 13.0$ corresponding to onset of the appearance of the EB effect under ZFC conditions. In Ni_2MnSn, the Heusler cell is composed

TABLE I. Magnetic moments and relative amount of AF exchange.

x	e/a	μ	% AF exchange
25.0	7.75	1.10	0
16.0	8.01	0.66	14.7
15.1	8.04	0.62	15.4
13.0	8.12	0.42	22.0
11.4	8.16	0.28	26.7
10.1	8.20	0.18	30.0
8.9	8.25	0.06	34.0
7.1	8.30	− 0.05	36.6
0	8.50	− 1.9	100

of 8 Ni, 4 Mn, and 4 Sn atoms. Replacing two of the four Sn atoms with Mn in each Heusler cell will allow the Mn atoms and along with it the AF exchange to percolate through the sample. The cell then consists of 8 Ni, 6 Mn, and 2 Sn atoms corresponding to the composition $Ni_{50.0}Mn_{37.5}Sn_{12.5}$. This is roughly the composition at which one begins to observe initial curves that lie outside the hysteresis loop and EB under ZFC conditions. For this composition, the amount of AF exchange contribution is about 24%, for which the AF exchange is strong enough with respect to the energy supplied by the applied field to maintain the prevailing spin configuration of the FM entities up to H_{crit}. This is verified by the reversibility of $M(H)$ up to H_{crit} as indicated in Fig. 2(b). Above this field, the dominance of the AF exchange on the FM configuration is overcome by the external field, and the FM alignment is reconfigured into a SF state irreversibly up to H_m. When the field is reduced from above H_m, the obtained loops are shifted negatively, as would be similar to the case when the system's spins are configured by a cooling field; namely, the FC case. Therefore, the observation of ZFC exchange bias relies initially on the reconfiguration of the FM spins in the interval $H_{crit} \leqslant H \leqslant H_m$ after which the AF exchange interacts with the reconfigured SF state to give rise to the EB effect. As the temperature increases, H_{crit} and H_m both decrease, and the EB effect diminishes.

A number of depictions describing the EB process are found in the literature from the first observation of the EB effect [8] to its more recent observations in martensitic Heuslers under ZFC conditions [21]. The latter describes the process of spin reconfiguration with a growth in the FM component when an external field is applied to a system in a SSG state. In the blocked state, as T_B reaches its maximum at about $(e/a) \approx 8.12$ FM coupling is relatively strong, and AF coupling is weak. In this case a reconfiguration of the ZFC state does not occur, and EB is not observed in the ZFC case. For $(e/a) > 8.12$, T_B begins to decrease, and AF exchange begins to percolate, whereas FM exchange begins to be confined to isolated regions. As the Mn concentration further increases, the volume of AF regions become larger in size at the expense of the size of the FM component. As the limit to the SSG state is approached, a magnetic configuration of FM regions embedded in a frustrated antiferromagnet is found, and the EB effect increases by about an order of magnitude as seen by comparing Figs. 3(b) and 5(b).

VI. CONCLUSION

Magnetization studies on $Ni_{50}Mn_{50-x}Sn_x$ martensitic Heusler compounds in the range between $13.0 \geqslant x \geqslant 8.9$ can exhibit EB properties under both FC and ZFC conditions below T_B. The ZFC EB effect arises when the initial spin configuration of the FM entities, pinned by the AF exchange of the matrix, is reconfigured into a SF state above H_{crit}. This state is then maintained, and its exchange interaction with the AF surrounding leads to a shifted hysteresis loop.

ACKNOWLEDGMENT

This work was supported by the Deutsche Forschungsgemeinschaft, SPP 1599.

[1] M. Acet, L. Mañosa, and A. Planes, in *Handbook of Magnetic Materials*, edited by K. H. J. Buschow (Elsevier, Amsterdam, 2011), Vol. 19, pp. 231–289.
[2] A. Çakır, L. Righi, F. Albertini, M. Acet, M. Farle, and S. Aktürk, J. Appl. Phys. **114**, 183912 (2013).
[3] S. Aksoy, M. Acet, P. P. Deen, L. Manosa, and A. Planes, Phys. Rev. B **79**, 212401 (2009).
[4] C. Mondelli, K. Andersen, H. Mutka, C. Payen, and B. Frick, Phys. B (Amsterdam, Neth.) **267–268**, 139 (1999).
[5] T. Fennell, P. P. Deen, A. R. Wildes, K. Schmalzl, D. Prabhakaran, A. T. Boothroyd, R. J. Aldus, D. F. McMorrow, and S. T. Bramwell, Science **326**, 415 (2009).
[6] S. Aksoy, O. Posth, M. Acet, R. Meckenstock, J. Lindner, M. Farle, and E. F. Wassermann, J. Phys.: Conf. Ser. **200**, 092001 (2009).
[7] M. Khan, I. Dubenko, S. Stadler, and N. Ali, Appl. Phys. Lett. **91**, 072510 (2007).
[8] W. H. Meiklejohn and C. P. Bean, Phys. Rev. **102**, 1413 (1956).
[9] J. Nogués, D. Lederman, T. J. Moran, and Ivan K. Schuller, Phys. Rev. Lett. **76**, 4624 (1996).
[10] M. Khan, I. Dubenko, S. Stadler, and N. Ali, J. Appl. Phys. **102**, 113914 (2007).
[11] V. Buchelnikov, V. Sokolovskiy, I. Taranenko, S. Taskaev, and P. Entel, J. Phys.: Conf. Ser. **303**, 012084 (2011).
[12] A. Çakır, M. Acet, and M. Farle, Phys. Status Solidi B **251**, 2120 (2014).
[13] S. Pramanick, S. Cattopadhyay, S. Giri, S. Majumdar, and S. Chatterjee, J. Appl. Phys. **116**, 083910 (2014).
[14] C. Tsang, R. E. Fontana, T. Lin, D. E. Heim, V. S. Speriosu, B. A. Gurney, and M. L. Williams, IEEE Trans. Magn. **30**, 3801 (1994).
[15] J. Nogués and Ivan K. Schuller, J. Magn. Magn. Mater. **192**, 203 (1999).
[16] S. S. P. Parkin, K. P. Roche, M. G. Samant, P. M. Rice, R. B. Beyers, R. E. Scheuerlein, E. J. O'Sullivan, S. L. Brown, J. Bucchigano, D. W. Abraham, Y. Lu, M. Rooks, P. L. Trouilloud, R. A. Wanner, and W. J. Gallagher, J. Appl. Phys. **85**, 5828 (1999).
[17] M. Bode, E. Y. Vedmedenko, K. von Bergmann, A. Kubetzka, P. Ferriani, S. Heinze, and R. Wiesendanger, Nat. Mater. **5**, 477 (2006).
[18] F. Nolting, A. Scholl, J. Stöhr, J. W. Seo, J. Fompeyrine, H. Siegwart, J.-P. Locquet, S. Anders, J. Lüning, E. E. Fullerton, M. F. Toney, M. R. Scheinfein, and H. A. Padmore, Nature (London) **405**, 767 (2000).
[19] I. Schmid, P. Kappenberger, O. Hellwig, M. J. Carey, E. E. Fullerton, and H. J. Hug, Europhys. Lett. **81**, 17001 (2008).
[20] Z. D. Han, B. Qian, D. H. Wang, P. Zhang, X. F. Jiang, J. L. Zhang, and Y. W. Du, Appl. Phys. Lett. **103**, 172403 (2013).
[21] B. M. Wang, Y. Liu, P. Ren, B. Xia, K. B. Ruan, J. B. Yi, J. Ding, X. G. Li, and L. Wang, Phys. Rev. Lett. **106**, 077203 (2011), and supplementary material.

[22] J. Sharma and K. G. Suresh, Appl. Phys. Lett. **106**, 072405 (2015).

[23] A. Çakır, L. Righi, F. Albertini, M. Acet, and M. Farle, Acta Mater. **99**, 140 (2015).

[24] J. S. Kasper and J. S. Kouvel, J. Phys. Chem. Solids **11**, 231 (1959).

[25] T. Krenke, M. Acet, E. F. Wassermann, X. Moya, L. Mañosa, and A. Planes, Phys. Rev. B **73**, 174413 (2006).